



Cite this: DOI: 10.1039/c8nr01968a

## Low-cost, flexible, disinfectant-free and regular-array three-dimensional nanopyramid antibacterial films for clinical applications†

Kwong-Hoi Tsui,<sup>‡a</sup> Xin Li,<sup>‡b,d</sup> James K. H. Tsoi,<sup>Ⓜc</sup> Siu-Fung Leung,<sup>a</sup> Tang Lei,<sup>a</sup> Wing Yi Chak,<sup>a</sup> Chengfei Zhang,<sup>b</sup> Jiang Chen,<sup>d</sup> Gary S. P. Cheung<sup>\*b</sup> and Zhiyong Fan<sup>Ⓜ\*a</sup>

In this work, a low-cost, scalable and highly repeatable approach was developed to prepare polystyrene films with three-dimensional nanopyramids on the surface. The nanopyramids have a tunable aspect ratio and more importantly, their anti-bacterial performance has been systematically studied. The effectiveness of the nanopyramids on *E. coli* growth inhibition and the role of the nanostructure aspect ratio were carefully studied through scanning electron microscopy and confocal laser scanning microscopy. The results showed an excellent antibacterial performance with more than 90% reduction in the *E. coli* population in all nanopyramid samples after a 168 h prolonged incubation time. The nanopyramid film developed here can be used for clinical and commercial applications to prevent the growth of pathogenic bacteria on various surfaces.

Received 17th March 2018,  
Accepted 16th April 2018  
DOI: 10.1039/c8nr01968a

rsc.li/nanoscale

### Introduction

Pathogenic bacteria have long been a threat to public health as they may cause morbidity and mortality. In recent years, the prevalence of multidrug-resistant bacteria has become a serious challenge in the clinical area.<sup>1–3</sup> It has been reported that traces of multidrug-resistant bacterial contamination can be easily found on inanimate surfaces and equipment in intensive care units (ICUs) and surgical wards.<sup>4–6</sup> In fact, medical equipment and high-contact communal surfaces such as computer keyboards, curtains, doors and floors are incubation sites for pathogenic biofilm formation. It was reported that both Gram-positive and Gram-negative bacteria can remain alive for months under humid and low temperature conditions.<sup>7</sup> Moreover, cross-transmission of bacteria from inanimate surfaces may play a significant role in ICU-acquired colonization and infections.<sup>7</sup> Traditionally, chemical-based disinfection is used to remove the bacteria on the surfaces.

However, regular cleaning with chlorine solution may not completely remove the multidrug-resistant bacteria containing biofilms on dry surfaces.<sup>4,8</sup> Furthermore, the chemical residue from the cleaning may be harmful to patients and the effectiveness does not last for a long period of time. Nanomaterials such as silver nanoparticles, silicon nanowires or carbon nanotubes have been proposed for antibacterial and biomedical applications<sup>7,9–17</sup> but the toxicity of these nanomaterials is pending for further evaluation.<sup>18,19</sup> Recently, the mechanobiological influence of micro/nanostructures on cells and bacteria has attracted much attention.<sup>20–22</sup> Nanostructured surfaces have been proven effective to inhibit the bacterial growth on the surfaces.<sup>8,23–31</sup> The main mechanism is based on a biophysical bactericidal model in which bacteria are neutralized by mechanical puncturing and rupturing without using any chemical agent.<sup>8,24–26,30–32</sup> A disinfectant-free bactericidal process is favorable for clinical applications because it can reduce the risk of chemical residue contamination. However, most of the potential bactericidal nanostructures are prepared on solid substrates such as silicon, titanium and aluminum because of the advance in photovoltaic devices in the past few decades.<sup>33–43</sup> It is difficult to apply them to the existing inanimate surfaces and equipment. In this regard, polymeric nanostructured films are promising alternatives because they can be readily attached to any surface as protection films of a window. However, current reports on using polymer nanostructures for bactericides are still limited by the small size of the nanostructured film, primarily prepared with a biotemplating method, in which the polymeric nanostructured surfaces are obtained from replicating the nanostructures from biospe-

<sup>a</sup>Department of Electronic and Computer Engineering, The Hong Kong University of Science and Technology, Clear Water Bay, Kowloon, Hong Kong SAR, China.

E-mail: eezfan@ust.hk

<sup>b</sup>Discipline of Endodontology, Faculty of Dentistry, The University of Hong Kong, Pokfulam, Hong Kong SAR, China. E-mail: spcheung@hku.hk

<sup>c</sup>Dental Materials Science, Faculty of Dentistry, The University of Hong Kong, Pokfulam, Hong Kong SAR, China

<sup>d</sup>Department of Oral Implantology, Affiliated Stomatological of Fujian Medical University, Fuzhou, Fujian 350002, China

†Electronic supplementary information (ESI) available. See DOI: 10.1039/c8nr01968a

‡These authors contributed equally to this work.

cies bodies, such as gecko skin.<sup>8,24–26,30,31</sup> The small size of the animal's body surface limits the size of the replicated film. Furthermore, the variations in the nanostructure geometry in the biospecies bodies hinder the development of a large-scale process because of the high-cost of body sampling and a complicated replication process.

In this work, we have utilized a facile molding process to prepare flexible polystyrene (PS) antibacterial films with three-dimensional (3D) nanopyramid arrays on the surface. The geometry of the nanopyramids, *i.e.*, their aspect ratio and pitch, can be precisely controlled by tuning the structure of the inverted nanopyramid template in the fabrication process. The antibacterial film can be easily attached to any surface such as curtains and walls in clinical wards to prevent the pathogenic bacteria from forming biofilms. The fabrication method can be further developed into a production scale process and the low-cost feature of polystyrene enables large scale utilization in clinical applications. Particularly, the antibacterial effectiveness on the Gram-negative bacterium *Escherichia coli* (*E. coli*) has been evaluated using scanning electron microscopy (SEM) and confocal laser scanning microscopy (CLSM). More than 90% reduction of *E. coli* colonization has been identified. The effectiveness can be maintained up to 168 hours without cleaning. Furthermore, by tuning the aspect ratio of inverted nanopyramid nanostructures, systematic investigation into the effect of nanopyramid geometry on the bactericidal performance has been performed. It was found that the sharper pyramid surface has a better antibacterial effect in the initial stage but the prolonged antibacterial effect is not as effective as that with the less sharp nanopyramid surface. This study helps to reveal the mechanism of the biophysical bactericidal effect with nanostructures.

## Experimental

### Fabrication of i-pyramid templates with different aspect ratios

A clean <100> oriented Si wafer with 100 nm thermally grown silicon oxide on the surface was spin-coated with a photoresist AZ7908 and patterned with photolithography to obtain a regular square array of pits with a pitch of 1.5  $\mu\text{m}$ . Then, the patterned wafer was etched with benzoxazolinone (BOA) to remove the exposed Si oxide layer, which functions as an etching mask in the subsequent i-pyramid formation. After removing the photoresist in acetone, the wafer was then put into the 15% tetramethylammonium hydroxide (TMAH) solution at 50  $^{\circ}\text{C}$  for 50 min. The highly regular array of inverted pyramids (i-pyramids) was formed by anisotropic etching of the patterned Si wafer. Finally, 400 nm, 800 nm or 1200 nm of chromium were sputtered to wafers respectively to adjust the aspect ratio of the i-pyramids using the Nano-master NSC3000 Sputtering System (SPT-NSC3000).

### Fabrication of nanopyramid films

Polystyrene (PS) with an average molecular weight of around 192 000 was purchased from Sigma Aldrich. The material (10 g) was dissolved in 100 mL of toluene to obtain a PS solu-

tion. Then, the solution was poured onto the i-pyramid wafer. The PS solution was first heat cured at 90  $^{\circ}\text{C}$  for 3 hours and then was held at 120  $^{\circ}\text{C}$  for the next 30 min. After that, the PS nanopyramid film was readily peeled off from the i-pyramid wafer, owing to the anti-sticking property of chromium. Groups of specimens, Nanopyramid type A (NPA), Nanopyramid type B (NPB) and Nanopyramid type C (NPC), are obtained corresponding to the nanopyramid films obtained from templates coated with 400 nm, 800 nm or 1200 nm of chromium respectively.

### Characterization and bacterial cell viability analysis

SEM images were obtained using a JEOL JSM-7100F SEM operated at 10 kV. The water contact angle was measured using a USA KINO contact angle meter SL200KB with a water droplet volume of 5  $\mu\text{L}$ . For the bacterial cell viability analysis, confocal laser scanning microscopy (CLSM) was carried out to visualize the relative proportion of live and dead cells on the nanopyramid surface after staining with the LIVE/DEAD BacLight Bacterial Viability Kit (L-7012 Invitrogen, Molecular Probes, Eugene, OR, USA) according to the manufacturer's protocol. This proprietary staining kit contains a mixture of SYTO 9 and propidium iodide fluorescent dyes that make live bacteria show up in green and dead bacteria in red color. Nine randomly assigned regions of each specimen with a field dimension of 200  $\mu\text{m}$   $\times$  200  $\mu\text{m}$  were imaged using a CLSM (IX81 FluoView FV1000, Olympus, Tokyo, Japan). All CLSM images were imported into the computer and the amount of live and dead bacterial cells on the surfaces was determined using the image analysis software (ImageJ, National Institute of Health, Bethesda, Maryland, USA).

## Results and discussion

The inverted nanopyramid arrays were prepared on a <100> oriented silicon (Si) substrate with the aspect ratio of the i-pyramids adjusted by depositing different layers of Cr with different thicknesses at a certain position, as mentioned in the Experimental section. This chromium-sputtered array becomes the negative template for molding with polystyrene (PS) solution to obtain flexible nanopyramid films. Note that PS is a low cost, widely used plastic in our daily life. It is commonly used in the form of containers in clinical applications. On the other hand, other plastic materials, such as PMMA, polycarbonate, *etc.*, can also be molded with a similar approach, allowing a wide choice of material to satisfy various practical requirements in clinical applications. Fig. 1a–d show the schematics of the i-pyramid template fabrication process. The detailed fabrication process is shown in the Experimental section. Dimensions of the i-pyramid were controlled by the etching time, however all of them have a fixed aspect ratio (ratio of height to width) of 1.41 because of the unique anisotropic etching property of Si.<sup>44</sup> In order to modulate the aspect ratio of the i-pyramid, 400 nm, 800 nm and 1200 nm of chromium were sputtered to wafers (see Fig. 1e–g). The i-pyramid

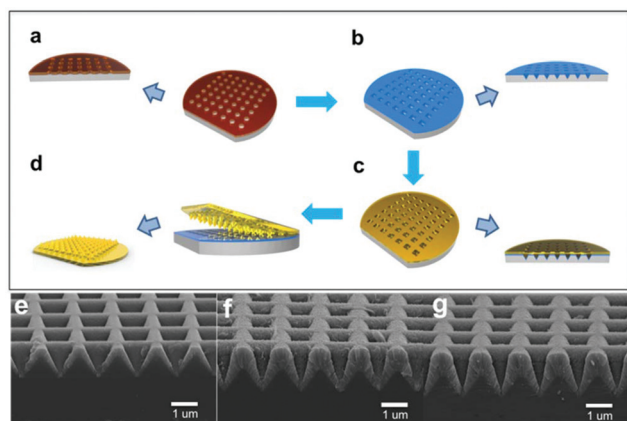


**Fig. 1** Schematics of the nanopillar fabrication process and SEM images of inverted pyramid templates. (a) A  $\langle 100 \rangle$  oriented Si wafer with a 100 nm  $\text{SiO}_2$  substrate underwent photolithography with a  $1.5 \mu\text{m}$  square array pattern and BOA etching. (b) The patterned wafer underwent TMAH etching to form an i-pyramid template. (c) Different thicknesses of chromium sputtered on the surface. (d) Regular nanopillar on the PS film after peeling off. (e) 400 nm chromium sputtered template. (f) 800 nm chromium sputtered template. (g) 1200 nm chromium sputtered template.

became sharper with thicker Cr deposition. And the aspect ratio of i-pyramids also increased when thicker Cr was deposited. This is a unique approach to precisely modulate the aspect ratio of a regular array of i-pyramids at the nanoscale. To prepare the films (Fig. 1d), PS solution was poured on the surface of the templates. A transparent PS film with regular, positive, protruding nanopillars on its surface was obtained after directly peeling it off from the Si mold. The 3 groups of PS films, Nanopyramid type A (NPA), Nanopyramid type B (NPB) and Nanopyramid type C (NPC) represent the nanopillar films replicated from 400 nm, 800 nm and 1200 nm chromium sputtered templates respectively. A planar, microscopically smooth PS film was prepared by molding a polished, flat Si wafer as the control sample to compare the result with nanopillars. It is worth noting that the Cr layer also served very well as an anti-adhesive layer. This means that the template could be reused multiple times without any residual PS material left on its surface. Furthermore, multiple templates can be stitched together to an even larger template for the process. Compared to other reported approaches, such as casting and molding from gecko skin or cicada wing, the fabrication process described here is much more controllable and the nanostructured films are much more uniform. Potentially, large-scale and practical films can be easily prepared using this method.

With the process described above, the nanopillar PS films obtained have a number of distinct features that make them attractive as an antibacterial surface. Fig. 2a shows a photograph of the fabricated film with the surface nanopillar pattern with a size of  $7.5 \text{ cm} \times 7.5 \text{ cm}$ . The rainbow color from light diffraction indicates perfect ordering of nanostructures on the surface. Note that the current film size is

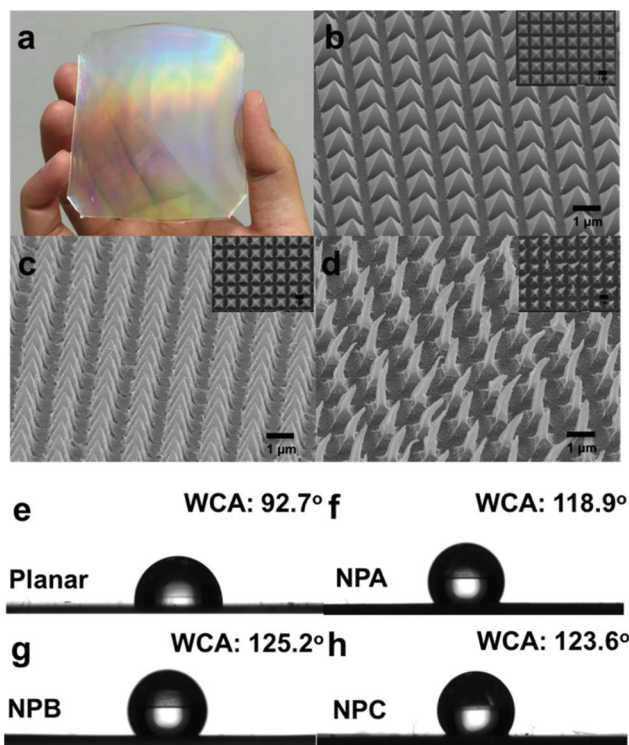


**Fig. 2** (a) Flexible PS nanopillar film. SEM image of the (b) NPA PS film, (c) NPB PS film and (d) NPC PS film. Water contact angle of the (e) planar PS film, (f) NPA PS film, (g) NPB PS film and (h) NPC PS film.

much larger than the duplicates from the pelts of shed gecko skin and cicada wing. More importantly, the reproduction of surface structures was more consistent and uniform, and this makes the film more useful for practical applications. In fact, the size of the film can be readily scaled up by stitching together multiple pieces of these nanostructured Si wafers. Here any optimised structure and shape may also be transferred into a metal mold for a manufacturing process. For example, a roll-to-roll hot-embossing process can be applied to produce a continuous nanostructured antibacterial film. Since the bacterial infection in the surgical site remains a critical issue, one potential application for these nanostructures is to integrate this nanopillar film into clinical instruments, catheters and containers that can remain bacteria-free for a prolonged period. Having a physical antibiotic surface means there is no need for use of toxic disinfectants and sterility maintenance. The material cost of plastic polymers for the biomedical applications is very low. Fig. 2b–d show the SEM images of the NPA, NPB and NPC PS films. The positive nanopillars with a pitch of  $1.5 \mu\text{m}$  were highly ordered and showed poor wetting (very high contact angle) by water. The highly ordered and tunable surface structures also provide an excellent and versatile platform to investigate interactions, at a small scale, between various nanotopography–geometry combinations and bacteria. There was wide-ranging selectivity for different morphologies provided by varying the thickness of

the Cr sputtered coating on the Si mold, which is an effective means to control the aspect ratio of the nanoscale structures. Therefore, by modulating the Cr thickness, the relief of the structures could be altered with increasing protuberance sharpness.

The water contact angle is one of the key factors that determines the bacterial adhesion on a surface.<sup>11,45–47</sup> Typically, a high water contact angle suggests a low surface energy. The lower the surface energy, the more difficult is the adhesion of bacteria to the surface. Therefore, the water contact angle is used to compare surfaces for their antibacterial potential. Fig. 2e–h show the water contact angles of the planar, NPA, NPB and NPC PS films, respectively. The water contact angle significantly increased from 92.7° to around 120° for those surfaces with nanopyramid structures. It can be easily understood by using Wenzel's model of wetting that the contact angle of the surface increased with the surface roughness.<sup>48</sup> The nanopyramid significantly increased the surface roughness compared to the planar sample. Therefore, the surface of the nano-patterned PS film was more hydrophobic compared to the smooth planar surface.

To verify the antibacterial effect of the nano-patterned surface, the three groups of molded PS films together with a smooth (non-textured control) sample were placed in an *Escherichia coli* (*E. coli*) suspension of concentration  $1 \times 10^9$  cells per mL. Four incubation times (1 hour, 24 hours, 72 hours and 168 hours) were examined in such an aqueous environment. Fig. 3 shows settling of the *E. coli* cells on the different surfaces of all four samples after 1, 24, 72, and 168 hours of incubation time. For the control surface, the *E. coli* cells attached to the surface, and the amount continued to increase with time (Fig. 3a, e, i and m). Bacterial aggregation in a highly organised manner is one of the key phenomena indicating biofilm formation.<sup>28,49</sup> In contrast, bacteria seemed incapable of settling on nano-patterned surfaces and they were not able to congregate to any significant degree.

Furthermore, the regular nanostructure arrays separated individual bacterium, trapping them between the protuberances, so that interaction between bacteria was significantly disturbed.<sup>8</sup> For surfaces with the nanostructures with the highest aspect ratio (e.g. on the NPC PS film (Fig. 3d, h, l and p)), it can be seen that bacteria were suspended on top of the nanostructure tips. The microscopic observation suggests that the nanopyramids are rigid enough, and they can prevent the bacterial cells from slipping down into the gap. However, some nano-spikes on the surface of the NPC PS film were bent, with those cells that had been punctured now situated on top of the tip. These cells formed clusters with neighboring dead cells also suspended at the tips of the adjacent nanostructures.<sup>23</sup> The 24-hour incubated samples showed the presence of intact bacteria on the planar (control) surface, with *de novo* elements of biofilm community formation (Fig. 3a, e, i and m). However, the result was clearly different in the nanostructured samples. Some bacteria appeared to have been shredded by the nanostructures (Fig. 3b–d, f–h, k, l and n–p). The higher the aspect ratio for the nanopryamid structures, the more the bacteria cells were ruptured and deceased. After the 72-hour and 168-hour incubation, the *E. coli* population increased in quantity significantly in the control sample, as expected (see Fig. 4), resulting in biofilm formation. In contrast, the majority of bacteria on those nano-patterned surfaces were shredded and ruptured (Fig. 3b–d, f–h, j–l and n–p).

Confocal laser scanning microscopy (CLSM) was used to quantify the effectiveness of bacteria annihilation on the different surfaces after 1, 24, 72 and 168 hours of *E. coli* incubation. A mixture of SYTO 9 and propidium iodide stains was used as the fluorescent dyes to visualize the live and dead

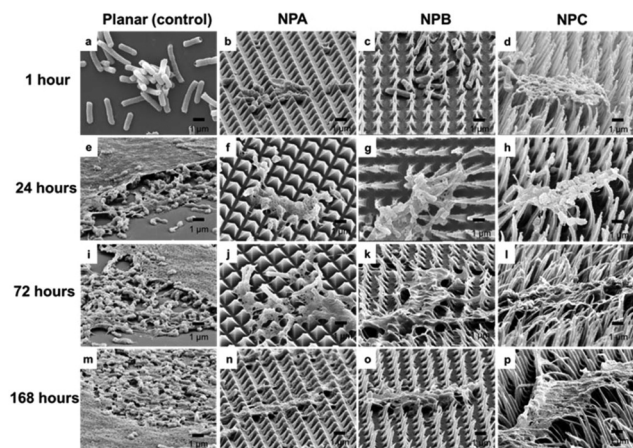


Fig. 3 SEM images of bacterial interaction with different samples for (a–d) 1-hour incubation time, (e–h) 24-hour incubation time, (i–l) 72-hour incubation time and (m–p) 168-hour incubation time. Scale bar: 1 μm.

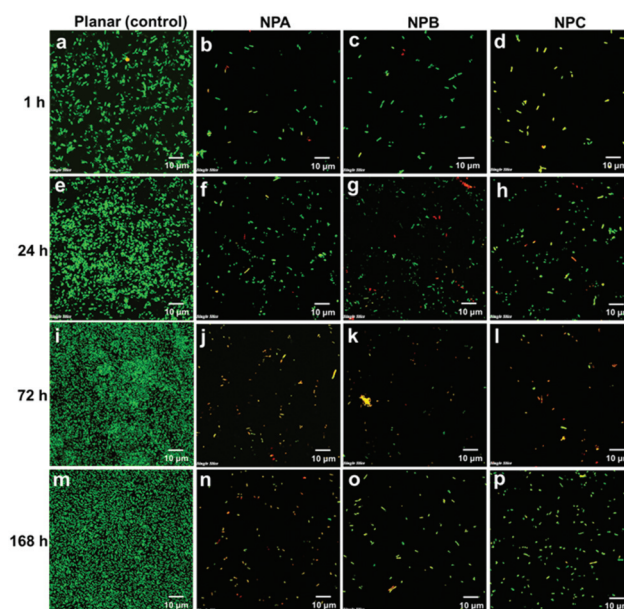


Fig. 4 CLSM images of live (green) and dead (red) fluorophore-tagged *E. coli* on the surface of different samples for 1-hour (a–d), 24-hour (e–h), 72-hour (i–l) and 168-hour (m–p) incubation time (per 200 × 200 μm<sup>2</sup>). Scale bar: 10 μm.

*E. coli* cells in CLSM. Cells with intact cell membranes stained green are considered to be viable while cells with damaged membranes stained red are considered to be non-viable. For the planar (control) sample, it could be clearly seen that the density of live *E. coli* cells increased with time in an exponential manner, and that an overwhelming majority of them remained vital and alive. Apparently, the surface density of cells on the flat surface is significantly greater than that on the nano-patterned surfaces throughout the period of incubation, regardless of the types of nanostructures, as shown in Fig. 4b–d, f–h, j–l and n–p. And CLSM fluorescence images also show that a significant quantity of dead bacteria can be observed. It is apparent that the growth and proliferation of *E. coli* are inhibited on the nanostructured surfaces.

To systematically analyze the bactericidal effect on all three types of nanostructures, namely NPA, NPB and NPC, the result from the confocal laser scanning microscopy is summarized in Fig. 5 and Table S1 in the ESI.† Fig. 5a shows the differential colonization of live *E. coli* on the nanostructured surfaces. It can be seen that on the planar sample, colonization by live *E. coli* increased from  $17.33 \times 10^3$  to  $59.38 \times 10^3$  cells per  $\text{cm}^2$  over 24 hours, but that then decreased to  $26.56 \times 10^3$  cells per  $\text{cm}^2$  from the 24 h to 72 h incubation time. This might be caused by the limit imposed by bacteria's life cycle. The amount of bacteria increased again to 61.45 cells per  $\text{cm}^2$  at 168 hours, and the reason will be explained in the next paragraph.

Initially, *E. coli* cells adhered to the planar, smooth PS surface and then started the reproduction process so that the colonization rate increased exponentially in the first 24 hours. However, the life cycle of *E. coli* came to an end after 24 hours and hence the amount of live *E. coli* decreased. Compared to the planar control, the three nanostructured samples showed

excellent antibacterial performance. The colonization for live *E. coli* over 168 hours remained at a low level. Most of the specimens showed colonization below  $4.0 \times 10^3$  cells per  $\text{cm}^2$ . Generally speaking, the growth and attachment of live *E. coli* cells on the nanostructured surface was inhibited in the first 72-hours, after which the growth picked up again, but the amount remained very low compared with the control.

One explanation for the presence of some bacteria attaching onto the nanostructured surface might be that the “valleys” of the nanopatterns have been filled up and the nanostructures were flattened by some adherent dead bacteria; and some later arriving cells managed to grow on the flattened surface. The bactericidal effect was demonstrated by the nanostructured surface through the biophysical action (perforating and rupturing of the bacteria) at least in the first 72 hours. For longer periods of incubation, SEM images showed that the dead *E. coli* cells were plentiful within the gap of the nanostructures (Fig. 3j and p). The flattened area permitted new bacteria to attach and grow.

The amount of dead *E. coli* that remained on the various surfaces is summarized in Fig. 5b. Colonization by dead *E. coli* cells was low, often with less than  $1.0 \times 10^3$  cells per  $\text{cm}^2$  in the first 72-hours of incubation, but it increased steadily with time on the nanostructured surface. The accumulation rate on the NPC surface is the fastest, reaching  $1.15 \times 10^3$  cells per  $\text{cm}^2$  after 72 hours and  $5.81 \times 10^3$  cells per  $\text{cm}^2$  after 168 h incubation, while that of the other two nanostructured samples is only around  $2.8 \times 10^3$  cells per  $\text{cm}^2$  after 168 h. This observation can be explained by the biophysical bactericidal mechanism of nanopillars. The attached *E. coli* was neutralized by being punctured and ruptured by the nanostructures and the annihilation rate depends on the sharpness of the nanopillars. The higher the aspect ratio for the nanostructures, the easier the *E. coli* cells are ruptured and annihilated on the surface. The NPC PS film had an outstanding bactericidal effect due to its highest aspect ratio among the three types of nanostructures, thus resulting in a greater amount of dead bacterial cells collected on that surface. On the planar sample, the least number of dead *E. coli* cells, about  $0.08 \times 10^3$  cells per  $\text{cm}^2$ , was found on the surface over 168 h incubation. There was a peak in the number of dead cells at 72 hours, which is due to the natural cell cycle (death) of *E. coli* as mentioned before.

The equation for the calculation of antibacterial is.

$$\text{Antibacterial efficiency (\%)} = \left( \frac{\text{No. of Live } E. coli \text{ in the control} - \text{No. of Live } E. coli \text{ in the sample}}{\text{No. of Live } E. coli \text{ in the control}} \right) \times 100\% \quad (1)$$

Besides studying the exact number of live and dead *E. coli* cells, it is also worthwhile to calculate the proportion of live *E. coli* cells in all the adhered bacteria, so that the bactericidal mechanism of the adhered bacteria could be studied. Fig. 5c shows the percentage of live *E. coli* cells among all the adhered bacteria. On the planar sample, over 97% of the adhered

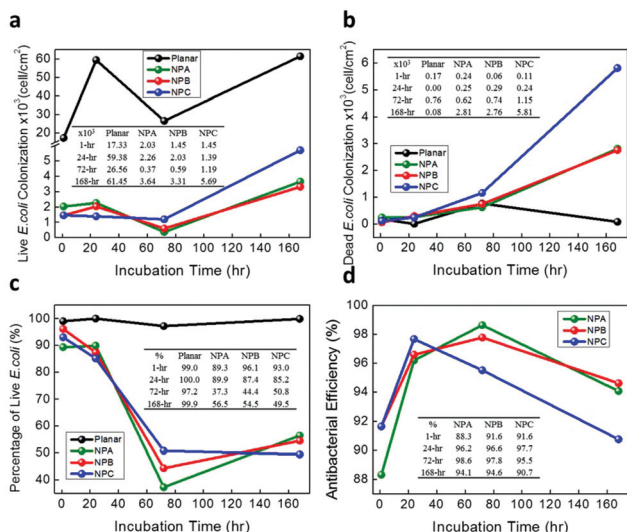


**Fig. 5** Summary of the CLSM results of different samples for different cell incubation times. (a) Live *E. coli* colonization. (b) Dead *E. coli* colonization. (c) Percentage of live *E. coli* occupied in the total number of adhered *E. coli*. (d) Antibacterial efficiency of different nano-patterned samples against living *E. coli* compared to the planar sample.

*E. coli* cells were alive within the 168 h incubation period. It implied that the planar PS surface had almost no bactericidal effect on the adhered *E. coli* cells. However, the result was totally different on nanopyramid surfaces. All samples showed a similar trend in the 168 h incubation period. Most of the adhered *E. coli* (around 90%) remained alive in the first 1 hour and it reduced to around 85% after 24 hours and continued to decline to below 50% after 72 hours. Then, the proportion of live and dead *E. coli* cells reached equilibrium to around 50% after 168 h incubation. It showed that biophysical bactericidal effect is not initiated in the initial stage when the *E. coli* just attaches to the nanostructured surfaces. However, the effect will gradually evolve with the increase in the adhesion time. Similar phenomena were also observed in our previous studies.<sup>8</sup> This trend coincided with our previously proposed mechanism of the mechanical destruction of adhered cells by gradual compression force added by surrounding nanostructures. At the end, the proportion of live and dead bacteria reached equilibrium in 168 h incubation. This is because some nanostructure areas were flattened by the dead bacteria and some of the new bacteria grew on the planar area without being killed. An equilibrium was achieved. Finally, the antibacterial performances of different surfaces were compared. The antibacterial performance of a nanostructured surface can be considered as the combinational effect of anti-adhesion and biophysical bactericidal in this study. Both effects gave the same result of reducing the number of live *E. coli* cells on the surface so that the growth of a biofilm was largely inhibited. The number of live bacteria on the surface could be used as the figure of merit to calculate the antibacterial efficiency of the nanostructured film compared to the planar sample as the control. The calculation method is shown in eqn (1). Fig. 5d shows the antibacterial efficiency of NPA, NPB and NPC at different incubation times. Most of the conditions showed an excellent antibacterial performance of >90% efficiency to prevent live bacteria on the surface. They showed a similar bell curve trend in the antibacterial performance. The efficiency increased initially to reach the peak and then decreased. Specifically, NPC reaches its best antibacterial efficiency of 97.7% at 24 h incubation and then progressively decreases to 90.7% at 168 h incubation time. NPA and NPB showed a more similar trend where they reached the peak at 72 h incubation to around 96% and decreased to around 94% at 168 h incubation but NPA started with a lower efficiency of 88.3% while NPB started with 91.6%. The trend could be explained by the progressive weakening of the combined action of anti-adhesion and the biophysical bactericidal effect with the incubation time. Both effects were weakened due to the flattening of nanostructures by adhered dead bacteria. The initial increase in the efficiency was mainly contributed to by the biophysical bactericidal effect as mentioned previously. The bactericidal effect dramatically dropped afterwards because the nanostructures were covered to form flattened surfaces. The performance was expected to further decrease after 168 h use. After all, the nanopyramid films definitely showed an excellent antibacterial performance compared to the planar surface.

## Conclusions

In summary, we have demonstrated a facile process to prepare large-scale, flexible nanostructured films with regular nano-engineered templates. It has been proved that these films possess an antibacterial effect and can inhibit the growth of biofilms on their surfaces. The antibacterial mechanism and performance were quantitatively examined by SEM and CLSM analyses. These nanostructured surfaces showed excellent and effective bactericidal performance with >90% reduction of *E. coli* colonization on the surface, compared with the control flat sample. Moreover, that effectiveness can be maintained up to 168 hours without cleaning. The reported nano-patterned films can be applied in clinical applications to reduce the risk of pathogenic infection.

## Conflicts of interest

There are no conflicts of interest to declare.

## Acknowledgements

This work was supported by the General Research Fund (project 16237816) from the Hong Kong Research Grant Council, the Hong Kong Innovation and Technology Fund (ITS/362/14FP and ITS/415/16) from the Innovation and Technology Commission and the Endodontic Research Fund of the Faculty of Dentistry, the University of Hong Kong (Account No.: 10212.200004107.012058.08008.400.1). We also acknowledge the Nanosystem Fabrication Facility (NFF) of HKUST for the nanofabrication.

## References

- 1 E. D. Brown and G. D. Wright, *Nature*, 2016, **529**, 336–343.
- 2 R. L. Finley, P. Collignon, D. J. Larsson, S. A. McEwen, X. Li, W. H. Gaze, R. Reid-Smith, M. Timinouni, D. W. Graham and E. Topp, *Clin. Infect. Dis.*, 2013, **57**, 704–710.
- 3 Y. Feng, W. Chen, Y. Jia, Y. Tian, Y. Zhao, F. Long, Y. Rui and X. Jiang, *Nanoscale*, 2016, **8**, 13223–13227, DOI: 10.1039/c6nr03317b.
- 4 H. Hu, K. Johani, I. B. Gosbell, A. Jacombs, A. Almatroudi, G. S. Whiteley, A. K. Deva, S. Jensen and K. Vickery, *J. Hosp. Infect.*, 2015, **91**, 35–44.
- 5 V. Russotto, A. Cortegiani, S. M. Raineri and A. Giarratano, *Journal Intensive care*, 2015, **3**, 54.
- 6 A. Kramer, I. Schwebke and G. Kampf, *BMC Infect. Dis.*, 2006, **6**, 130.
- 7 D. T. Schoen, A. P. Schoen, L. Hu, H. S. Kim, S. C. Heilshorn and Y. Cui, *Nano Lett.*, 2010, **10**, 3628–3632.
- 8 X. Li, G. Cheung, G. S. Watson, J. A. Watson, S. Lin, L. Schwarzkopf and D. Green, *Nanoscale*, 2016, **8**, 18860–18869.

- 9 M. Lv, S. Su, Y. He, Q. Huang, W. Hu, D. Li, C. Fan and S. Lee, *Adv. Mater.*, 2010, **22**, 5463–5467.
- 10 Z. Xiu, Q. Zhang, H. L. Puppala, V. L. Colvin and P. J. Alvarez, *Nano Lett.*, 2012, **12**, 4271–4275.
- 11 J. Li, T. Kleintschek, A. Rieder, Y. Cheng, T. Baumbach, U. Obst, T. Schwartz and P. A. Levkin, *ACS Appl. Mater. Interfaces*, 2013, **5**, 6704–6711.
- 12 P. Cai, W. R. Leow, X. Wang, Y. Wu and X. Chen, *Adv. Mater.*, 2017, **29**, 1605529, DOI: 10.1002/adma.201605529.
- 13 S. Wang, J. Sun, Y. Jia, L. Yang, N. Wang, Y. Xianyu, W. Chen, X. Li, R. Cha and X. Jiang, *Biomacromolecules*, 2016, **17**, 2472–2478, DOI: 10.1021/acs.biomac.6b00642.
- 14 Y. Tian, J. Qi, W. Zhang, Q. Cai and X. Jiang, *ACS Appl. Mater. Interfaces*, 2014, **6**, 12038–12045, DOI: 10.1021/am5026424.
- 15 J. Zimmerman, R. Parameswaran, G. Murray, Y. Wang, M. Burke and B. Tian, *Sci. Adv.*, 2016, **2**, 12.
- 16 S. Ou, R. Chung, L. Lin, Y. Chiang, C. Huang and K. Ou, *J. Alloys Compd.*, 2015, **629**, 362–367, DOI: 10.1016/j.jallcom.2014.12.158.
- 17 R. Chung, M. Hsieh, C. W. Huang, L. H. Perng, H. Wen and T. Chin, *J. Biomed. Mater. Res., Part B*, 2006, **76**, 169–178, DOI: 10.1002/jbm.b.30365.
- 18 S. Sharifi, S. Behzadi, S. Laurent, M. L. Forrest, P. Stroeve and M. Mahmoudi, *Chem. Soc. Rev.*, 2012, **41**, 2323–2343.
- 19 L. Y. T. Chou and W. C. W. Chan, *Nat. Nanotechnol.*, 2012, **7**, 416–417, DOI: 10.1038/nnano.2012.110.
- 20 B. Hu, W. Shi, Y. Wu, W. R. Leow, P. Cai, S. Li and X. Chen, *Adv. Mater.*, 2014, **26**, 5786–5793, DOI: 10.1002/adma.201402489.
- 21 B. Hu, W. R. Leow, S. Amini, B. Nai, X. Zhang, Z. Liu, P. Cai, Z. Li, Y. Wu, A. Miserez, C. T. Lim and X. Chen, *Adv. Mater.*, 2017, **29**, 1700145.
- 22 B. Hu, W. R. Leow, P. Cai, Y. Li, Y. Wu and X. Chen, *ACS Nano*, 2017, **11**, 12302, DOI: 10.1021/acsnano.7b06063.
- 23 E. P. Ivanova, J. Hasan, H. K. Webb, G. Gervinskas, S. Juodkazis, V. K. Truong, A. H. Wu, R. N. Lamb, V. A. Baulin, G. S. Watson, J. A. Watson, D. E. Mainwaring and R. J. Crawford, *Nat. Commun.*, 2013, **4**, 2838, DOI: 10.1038/ncomms3838.
- 24 S. Pogodin, J. Hasan, V. A. Baulin, H. K. Webb, V. K. Truong, T. H. P. Nguyen, V. Boshkovikj, C. J. Fluke, G. S. Watson and J. A. Watson, *Biophys. J.*, 2013, **104**, 835–840.
- 25 G. S. Watson, D. W. Green, L. Schwarzkopf, X. Li, B. W. Cribb, S. Myhra and J. A. Watson, *Acta Biomater.*, 2015, **21**, 109–122.
- 26 J. Hasan, R. J. Crawford and E. P. Ivanova, *Trends Biotechnol.*, 2013, **31**, 295–304.
- 27 S. M. Kelleher, O. Habimana, J. Lawler, B. O'Reilly, S. Daniels, E. Casey and A. Cowley, *ACS Appl. Mater. Interfaces*, 2015, **8**, 14966–14974.
- 28 A. Epstein, A. Hochbaum, P. Kim and J. Aizenberg, *Nanotechnology*, 2011, **22**, 494007.
- 29 K. Suh, A. Khademhosseini, P. Yoo and R. Langer, *Biomed. Microdevices*, 2004, **6**, 223–229, DOI: 10.1023/B:BMMD.0000042052.47444.9a.
- 30 E. P. Ivanova, J. Hasan, H. K. Webb, V. K. Truong, G. S. Watson, J. A. Watson, V. A. Baulin, S. Pogodin, J. Y. Wang and M. J. Tobin, *Small*, 2012, **8**, 2489–2494.
- 31 E. P. Ivanova and R. J. Crawford, SpringerLink (Online service) and s. LINK (Online), in *Antibacterial surfaces*, Springer, Cham, Ger., 2015.
- 32 X. Li, *Phys. Chem. Chem. Phys.*, 2016, **18**, 1311–1316.
- 33 Z. Fan, H. Razavi, J. Do, A. Moriwaki, O. Ergen, Y. Chueh, P. W. Leu, J. C. Ho, T. Takahashi and L. A. Reichertz, *Nat. Mater.*, 2009, **8**, 648.
- 34 Z. Fan, D. Ruebusch, A. Rathore, R. Kapadia, O. Ergen, P. Leu and A. Javey, *Nano Res.*, 2009, **2**, 829–843, DOI: 10.1007/s12274-009-9091-y.
- 35 S. F. Leung, L. Gu, Q. Zhang, K. H. Tsui, J. M. Shieh, C. H. Shen, T. H. Hsiao, C. H. Hsu, L. Lu, D. Li, Q. Lin and Z. Fan, *Sci. Rep.*, 2014, **4**, 4243, DOI: 10.1038/srep04243.
- 36 H. Lin, F. Xiu, M. Fang, S. Yip, H. Cheung, F. Wang, N. Han, K. S. Chan, C. Wong and J. C. Ho, *ACS Nano*, 2014, **8**, 3752–3760.
- 37 K. Tsui, Q. Lin, H. Chou, Q. Zhang, H. Fu, P. Qi and Z. Fan, *Adv. Mater.*, 2014, **26**, 2805–2811.
- 38 M. Yu, Y. Long, B. Sun and Z. Fan, *Recent advances in solar cells based on one-dimensional nanostructure arrays*, 2012.
- 39 M. M. Tavakoli, Q. Lin, S. Leung, G. C. Lui, H. Lu, L. Li, B. Xiang and Z. Fan, *Nanoscale*, 2016, **8**, 4276–4283, DOI: 10.1039/c5nr08836d.
- 40 X. Zheng, Z. Wei, H. Chen, Q. Zhang, H. He, S. Xiao, Z. Fan, K. S. Wong and S. Yang, *Nanoscale*, 2016, **8**, 6393–6402, DOI: 10.1039/c5nr06715d.
- 41 H. Wu, C. Xu, J. Xu, L. Lu, Z. Fan, X. Chen, Y. Song and D. Li, *Enhanced supercapacitance in anodic TiO<sub>2</sub> nanotube films by hydrogen plasma treatment*, 2013, **24**, p. 455401, DOI: 10.1088/0957-4484/24/45/455401.
- 42 R. Yu, K. Ching, Q. Lin, S. Leung, D. Arcrossito and Z. Fan, *ACS Nano*, 2011, **5**, 9291–9298, DOI: 10.1021/nn203844z.
- 43 J. Lee, B. Hua, S. Park, M. Ha, Y. Lee, Z. Fan and H. Ko, *Nanoscale*, 2013, **6**, 616–623, DOI: 10.1039/c3nr04752k.
- 44 S. Franssila, *Introduction to microfabrication*, John Wiley & Sons, 2010.
- 45 A. Han, J. K. Tsoi, F. P. Rodrigues, J. G. Leprince and W. M. Palin, *Int. J. Adhes. Adhes.*, 2016, **69**, 58–71.
- 46 G. Bruinsma, H. Van der Mei and H. Busscher, *Biomaterials*, 2001, **22**, 3217–3224.
- 47 W. G. Characklis and K. C. Marshall, *Biofilms*, Wiley, New York, New York, 1990.
- 48 R. J. Crawford and E. P. Ivanova, *Superhydrophobic surfaces*, Elsevier, Amsterdam, Netherlands, 2015.
- 49 G. Feng, Y. Cheng, S. Wang, D. A. Borca-Tasciuc, R. W. Worobo and C. I. Moraru, *NPJ Biofilms Microbiomes*, 2015, **1**, 15022.